

# The complex picture of HD 24712:

## First magnetic Doppler images of a roAp star

T. Lüftinger<sup>1</sup>, O. Kochukhov<sup>2</sup>, T. Ryabchikova<sup>1,3</sup>, W.W. Weiss<sup>1</sup>, I. Ilyin<sup>4</sup>

<sup>1</sup> Institut für Astronomie, Universität Wien, Türkenschanzstrasse 17, 1180 Wien, Austria

<sup>2</sup> Department of Astronomy and Space Physics, Uppsala University Box 515, SE-751 20 Uppsala, Sweden

<sup>3</sup> Institute of Astronomy, Russian Academy of Sciences, Pyatnitskaya 48, 119017 Moscow, Russia

<sup>4</sup> Astrophysikalisches Institut Potsdam, An der Sternwarte 16, D-14482 Potsdam, Germany

**Abstract.** We present the first analysis of the structure of the surface magnetic field of a rapidly oscillating Ap (roAp) star. We deduce information about magnetic field geometry and abundance distributions of a number of chemical elements on the surface of the hitherto best studied roAp star, HD 24712, using an elaborate magnetic Doppler Imaging (MDI) code (Piskunov et al. 2002, Kochukhov et al. 2002), INVERS10, which allows to reconstruct simultaneously and consistently the magnetic field geometry and elemental abundance distributions on a stellar surface without any a priori assumptions. For this purpose we analysed time series spectra obtained in Stokes I and V parameters with the SOFIN polarimeter and recover surface abundance structures of sixteen different chemical elements, respectively ions, including Mg, Ca, Sc, Ti, Cr, Fe, Co, Ni, Y, La, Ce, Pr, Nd, Gd, Tb, and Dy. We find and confirm a clear dipolar structure of the surface magnetic field and unexpected correlation of elemental abundance to this field: one group of elements accumulates solely at the phase of maximum magnetic field strength, whereas the other group avoids this region and is enhanced around minimum magnetic field. We also observe relative shifts of abundance enhancement or depletion regions between the various elements exhibiting otherwise similar behaviour. We compare our results to detailed pulsational analysis of high quality spectroscopic data and to photometry from space. Recent theoretical investigations (Cunha 2006) give rise to the possibility of relating the shifts mentioned above to the influence of the magnetic geometry on pulsational phase shifts.

**Key words:** stars: atmospheres – stars: chemically peculiar – stars: individual: HD 24712 – stars: magnetic field geometry – stars: surface abundance structures

## 1 Introduction

Many physical processes important for stellar evolution are crucially influenced by stellar magnetic fields. Theoretical and observational frameworks tell us for instance that they influence microscopic diffusion of chemical elements within stellar interiors and they may also redistribute angular momentum or give rise to enhanced hydrodynamical instabilities and thus modify mixing properties in stellar interiors.

Ap stars, representing about 10% to 20% of the upper main sequence stars, exhibit magnetic fields that appear to be highly ordered, very stable, and often very strong. Many Ap stars also show dramatic line profile variations synchronized to stellar rotation, which is attributed to oblique magnetic and pulsation axes, and to the presence of a non-uniform distribution of chemical elements on their surface. Such inhomogeneities exist only in the atmospheres of A stars with magnetic fields, demonstrating that these fields play a crucial role in their formation and evolution.

The spectra of Ap stars also exhibit a remarkable variety of, often unidentified, spectral line features. Ryabchikova et al. (2004) for example find overabundances of up to a few dex for some iron peak and especially the second ionization stage of the rare earth elements (REE), while other chemical elements are found to be underabundant compared to the solar value.

An important subgroup of the Ap stars, the rapidly oscillating Ap stars, in addition exhibits high-overtone, low-degree, non-radial  $p$ -mode pulsations with periods of 6–21 minutes. Their projected pulsational amplitudes are modulated according to their visible magnetic field structure, which indicates a close connection between the magnetic field and the (currently unknown) pulsation mechanism.

The mentioned chemical peculiarities are attributed to the selective diffusion of ions under the influence of a magnetic field, possibly in combination with a weak, magnetically directed wind (see e.g., Babel 1992).

We focus our research on roAp stars since these objects exhibit a number of new, largely unexplored phenomena related to their pulsational variability, while sharing all the properties of other Ap stars. The roAp stars are the only main sequence stars in which high-overtone  $p$ -mode pulsations are easily detected and pulsation modes can be identified. Furthermore, roAp stars represent the only group of pulsating stars, for which magnetic and rotation characteristics can well be constrained observationally. Consequently, peculiar pulsating stars are key objects in the investigation of atmospheric and internal structure of the middle main sequence stars.

Still very little is known about the origin and structure of magnetic fields and their connection and interaction with surface abundance patches and pulsation. With the development of high-resolution spectropolarimeters it has become possible to extract the full amount of information about magnetic field and abundance distributions using Stokes parameter observations and applying magnetic Doppler imaging.

We have developed and tested a code for magnetic Doppler imaging (Piskunov et al. 2002; Kochukhov et al. 2002) that allows to reconstruct simultaneously and consistently the magnetic field vector and abundance distribution of various elements on a stellar surface by taking into account all relevant physics of polarized line formation. In deriving the surface abundances of numerous light, iron-peak and rare earth elements by applying magnetic Doppler imaging, we get more insight in the relation and interaction of magnetic fields, vertical and horizontal abundance characteristics and pulsation and thus in the atmospheric structure of Ap and roAp stars.

## 2 HD 24712

HD 24712 (HD1217, DO Eri) is the best studied roAp star with light (Wolff & Morrison 1973), spectrum and magnetic variations (considering this analysis, maybe, apart from the Sun, even the best or in most variety studied star), that was discovered to be a pulsator by Kurtz in 1982 (1982). Matthews et al. (1988) found radial velocity variations with an amplitude of  $0.4 \pm 0.05 \text{ km s}^{-1}$  and the main photometric period of 6.14 min.

During an observing campaign with the Whole Earth Telescope (WET), Kurtz et al. (2002) detected a ‘missing’ mode, where the detailed investigations by Cunha et al. (2003 and 2006) in this context suggest, that the  $p$ -mode pulsations are strongly affected by the global stellar magnetic field. The outstanding variations of rare earth lines give rise to the assumption, that these

Table 1: Basic physical parameters of HD 24712.

$T_{\text{eff}}$	$7350 \pm 150 \text{ K}$
$\log g$	$4.2 \pm 0.1$
$M$	$1.63 M_{\odot}$
$L/L_{\odot}$	$0.91 \pm 0.04$
$P_{\text{rot}}(d)$	$12.45877 \pm (16)$
$P_{\text{puls}}$	$\simeq 6.15$
$v_e \sin i$	$5.6 \text{ km s}^{-1}$

elements are concentrated in a thin layer where pulsation reaches its maximum amplitude. In addition, high spectrum resolution data (Ryabchikova et al. 2000) indicated indeed strong abundance concentrations of iron peak and rare earth elements on the surface of roAp stars.

These observational findings and a possible correlation to theoretical investigations made HD 24712 an ideal candidate for novel spectroscopic and spectropolarimetric observations with outstanding ground-based equipment to obtain:

- high resolution, high signal-to-noise ratio spectropolarimetric data with SOFIN at NOT
- high resolution, high quality time resolved spectra with UVES at VLT, simultaneously with
- high precision photometric observations from space with the MOST (Microvariability and Oscillation of Stars) satellite. This Canadian photometric space telescope (Walker et al. 2003) is a 15-cm Maksutov optical telescope, that feeds twin CCD detectors through a broadband filter (350–700 nm) and possesses a pointing accuracy better than  $\pm 1''$  rms (Walker et al. 2003). With this equipment it is possible to obtain rapid photometry of bright stars for up to 2 months and with nearly a 100% duty cycle.

The basic physical parameters of HD 24712 are listed in Table 1. The temperature was determined using the new stellar model atmosphere code LLMODELS (Shulyak et al. 2004), which allows to account for individual elemental abundances already during model atmosphere calculations;  $\log g$  was applied as derived by Ryabchikova et al. (1997)

### 3 Observations and Data Reduction

#### 3.1 Spectropolarimetry

Spectropolarimetric observations of HD 24712 were carried out in 2003, between Oct. 29 and Nov. 18., using the high resolution échelle spectrograph SOFIN attached to the Cassegrain focus of the 2.56 m Nordic Optical Telescope (NOT), La Palma, Spain. The spectrograph is equipped with three different cameras and to obtain observations in the spectropolarimetric mode, the second camera with a nominal resolving power of  $\approx 80\,000$  was used. 49 different spectral lines from seven spectral orders, each covering about 40 Å to 50 Å between 4000 and 6000 Å were used for magnetic Doppler imaging.

The polarized spectra were obtained with a Stokes polarimeter, consisting of a fixed achromatic quarter-wave plate, a beam splitter consisting of a calcite plate, and an achromatic rotating quarter-wave plate. The position of the quarter-wave plate is controlled by a stepping motor. Usually a sequence of four subexposures is processed in order to obtain accurate circular polarization measurements, where each of the beams is exposed twice, with the quarter-wave plate rotated by  $90^\circ$

after the first and before the last exposure. This way it is possible to reduce instrumental effects to a minimum, as in the images taken with the quarter-wave plate rotated by  $90^\circ$ , possible instrumental signatures change sign and cancel during the averaging of the two exposures.

For data reduction, the '4A' software package written in C (Ilyin 2000) was used. All standard procedures, like bias subtraction, flat field correction, subtraction of the scattered light, weighted extraction of the orders, and bad pixel (cosmic ray) corrections were included, and ThAr exposures obtained before and after each observing night were used to perform wavelength calibration and to test for possible spurious instrumental polarization, caused e.g. by bending of the spectrograph which is directly mounted on the telescope, different positions of the star on the slit, or temporal variations of the seeing. S/N ratios for the observed spectra typically reached 200–300.

Rotation phases of HD 24712 (see Table 2) were calculated according to the ephemeris and rotation period obtained by Ryabchikova et al. (2005):

$$\text{HJD}(\langle B_z \rangle_{max}) = 2453235.18(40) + 12.45877(16) \text{ d.}$$

Table 2: Journal of spectropolarimetric observations of HD 24712.

HJD (245 0000+)	Stokes Parameters	Rotational phases
2941.6516	I V	0.4396
2943.6341	I V	0.6001
2945.5758	I V	0.7562
2946.5973	I V	0.8380
2947.6067	I V	0.9171
2948.6514	I V	0.0026
2952.6267	I V	0.3207
2953.6572	I V	0.4040
2954.6316	I V	0.4824
2955.6350	I V	0.5620
2956.5954	I V	0.6390
2957.5958	I V	0.7204
2961.6160	I V	0.0414

### 3.2 Time series observations

High time resolved observations were obtained in 2001 and 2002 with the single-order  $f/4$  *GECKO* coude spectrograph and the EEV1-CCD at the 3.6-m *Canada-France-Hawaii* telescope with a resolving power of about 115 000. The observations covered seven spectral regions, containing the most interesting spectral lines of singly and doubly-ionized rare earth elements,  $\text{H}\alpha$ ,  $\text{H}\beta$ ,  $\text{O I}$ ,  $\text{Fe I}$ ,  $\text{Ca I}$ , and  $\text{Ba II}$ .

During the observing run for the spectropolarimetric data, another set of observations was obtained with the SOFIN high resolution échelle spectrograph on Nov. 6, 2003, with a nominal resolving power of  $\approx 80\,000$ .

The spectroscopic observations carried out in *parallel* to the MOST observing run were performed with the HARPS (High Accuracy Radial velocity Planet Searcher) spectrometer at the 3.6-m telescope at ESO, La Silla (resolving power of 120 000), and with the UVES spectrograph at the 8.2-m telescope, UT2 (Kueyen), of the VLT on Paranal, Chile, in Director's Discretionary Time (274.D-5011) and with a resolving power of about 80 000.

Further spectra during the MOST observations of HD 24712 were registered in Nov. 14/15, 2004, and on Dec. 01/02, 2004, with the high resolution spectrograph SARG at the 3.55-m *Telescopio Nazionale Galileo* (TNG) at the Observatorio del Roque de los Muchachos (La Palma, Spain), exhibiting a resolving power of about 57 000.

### 3.3 Photometric observations with the MOST satellite

MOST observed HD 24712 continuously for 30 nights, from Nov. 5, to Dec. 4, 2004, in parallel to the ground-based observing campaign that was organized by us to obtain the spectroscopic time series mentioned above.

While our investigations in time resolved spectroscopy were published recently (Ryabchikova et al. 2006), and the main photometric results will be published elsewhere (e.g. this conference, Matthews et al. 2006), we investigate here the results from our magnetic Doppler imaging analysis.

## 4 Magnetic Doppler Imaging (MDI)

Doppler imaging (DI) has become a very successful tool to gain information on inhomogeneities on the surface of a rotating star caused by changing abundance and/or magnetic field structure. By inverting time series of spectropolarimetric observations of rotating stars based on complex mathematical procedures implemented in INVERS10, the first MDI code, developed by Piskunov & Kochukhov (2002), it became possible to invert simultaneously the information of the rotationally modulated *Stokes profiles* into elemental abundance and the three vector components of the stellar magnetic field. In their Papers I and II, Piskunov & Kochukhov (2002) and Kochukhov & Piskunov describe in detail the concept of MDI, the basic numerical techniques like how to efficiently solve the magnetic radiative transfer, the surface integration of the resulting Stokes profiles and the application of the regularization concept.

In the case of HD 24712, observations in Stokes parameters I and V could be used for Mapping. Thus the *multipolar regularization* procedure had to be applied, as during the inversions an ill-posed problem has to be solved when using only circular Stokes parameters. Multipolar regularization (see Kochukhov & Piskunov 2002) introduces external constraints similar to the multipolar field parameterization proposed by Bagnulo et al. (1999) and leads INVERS10 to solutions close to a general second-order multipolar expansion, which enables reliable imaging of stars with quasi-dipolar or quadrupolar magnetic fields (Kochukhov & Piskunov 2002).

The additional information content of the Stokes profiles, compared to the data used for conventional Doppler Imaging, makes it possible to map also stars with rotational velocities as low as that of HD 24712 with  $v_e \sin i = 5.6 \text{ km s}^{-1}$ .

### 4.1 Magnetic field geometry

Determining the geometry of the magnetic field on the surface of HD 24712 was performed choosing seven different Fe I and five different Nd III lines, which are listed in Table 3. These lines were chosen because their mean Landé factors enable strong polarization signatures, they are not affected by severe blending, and they show clear variations in the strength of the Stokes I profiles.

Important parameters needed as input for the ZDI procedure are the tilt and the azimuth angle of the stellar rotational axis,  $i$  and  $\Theta$ . Bagnulo et al. (1995) determined, based on traditional circular- and on broadband linear polarization observations, both angles and found:

$$i = 137^\circ \text{ and } \Theta = 4^\circ.$$

Adopting these values, a clear dipolar geometry yielded the best fit to the observed line profiles. The

magnetic field strength varies between +2.2 kG and +4.4 kG. In Figures 3 and 4, the line profiles of the chosen Fe and Nd III lines (black dots), the according fit reached during the inversions (blue lines) and the resulting magnetic field geometry are presented. The dipolar structure agrees very well with the dipolar model proposed by Bagnulo et al. (1995), only differing in the polar field strength, where they obtain  $B_p = 3.9$  kG, compared to +4.4 kG derived from magnetic Doppler Imaging.

## 4.2 Iron and neodymium III abundance distribution

The surface abundances of Fe I and Nd III mapped simultaneously with the Stellar magnetic field geometry are shown in Fig. 2. As mentioned above, we were able to use seven different Fe I and five different Nd III lines listed in Table 3. It can be clearly seen, that abundances of both elements are quite globally structured. Fe varies between  $-5.2$  and  $-4.7$  dex, in its maximum, still slightly underabundant compared to the solar value ( $-4.59$  dex). Nd III follows the roAp pattern (Ryabchikova et al. 2001) of extreme overabundance of the second irons of the REE, and it varies between  $-8.0$  and  $-7.0$  dex (compared to  $-10.59$  dex solar value). Fe I and Nd III seem to be perfectly anticorrelated: Fe I is accumulated, where Nd III is depleted, and minimum Fe I abundance can be found, where Nd III is at its maximum.

Comparing the patterns of these two elements to the derived magnetic field geometry presented in Figure 4, we find that the Fe abundance enhancement region is associated with the area of minimum magnetic field strength around  $\phi \simeq 0.5$ , whereas the Nd III map exhibits its area of maximum abundance around the magnetic field maximum, where the positive magnetic pole is orientated towards the observer. Due to the orientation of the star we are not able to directly observe the negative magnetic pole.

It is surprising to see that, against expectations, both elements are not accumulated or depleted on *both* magnetic poles or around the *magnetic equator*. Furthermore, the center of maximum or minimum abundance, respectively, seems to be shifted in latitude and/or longitude with respect to the magnetic polar regions, not only for Nd, but also for several other elements presented in Section 4.3.

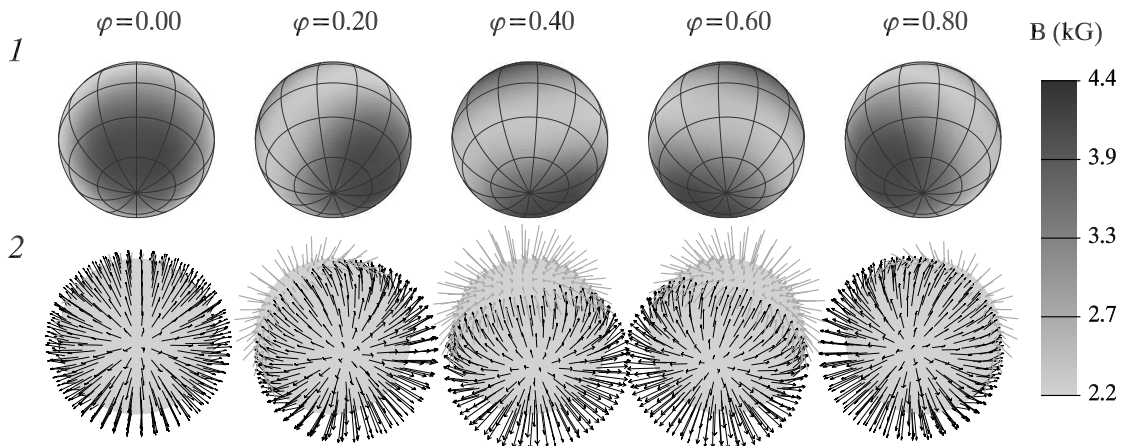


Figure 1: First mapping of the distribution of magnetic field strength (a) and field orientation (b) on the surface of a roAp star, as derived with modelling the Stokes I and V parameter stellar observations of HD 24712. The results reveal a pure dipolar magnetic field geometry on the surface of this star with a polar field strength varying between +2.2 kG and +4.4 kG.

Table 3: Table of elements and spectral lines used for mapping: type, spectral lines used, abundance interval and the range in dex, and the solar value for comparison are presented in columns from left to right.

Element	$\lambda$ (Å)	min, max $\log(N/N_{tot})$	abundance interval $\log(N/N_{tot})$	$\odot$ $\log(N/N_{tot})$
Magnesium I	5528	-5.9, -4.3	1.6	-4.51
Calcium II	5021	-5.2, -5.0	0.2	-5.73
Scandium II	5526	-10.1, -8.9	1.2	-8.99
Titanium II	4805 4911 5016	-7.8, -7.1	0.7	-7.14
Chromium II	5510	-6.1, -5.9	0.2	-6.40
Iron I	5505 5506 5242 5263 5267 5383 5397	-5.2, -4.7	0.5	-4.59
Cobalt I	4813 4897 5146 5250 5378 5393	-6.3, -5.8	0.3	-7.12
Nickel I	5035 5146	-7.6, -6.3	1.3	-5.81
Yttrium II	5119 5402	-9.0, -8.5	0.5	-9.83
Lanthanum II	4804 4808 4921 5377	-9.7, -8.8	0.9	-10.91
Cerium II	5117 5274	-9.3, -8.9	0.4	-10.46
Praseodymium II	5135	-10.0, -9.6	0.4	-11.33
Praseodymium III	4910 4929	-8.4, -7.7	0.7	
Neodymium II	4811 5033 5132 5143 5276 5361 5385 5399	-9.2, -8.5	0.7	-10.59
Neodymium III	4796 4821 4911 4912 4927	-8.0, -7.0	1.0	-10.59
Gadolinium II	5500	-8.8, -8.5	0.3	-10.92
Terbium III	5505	-8.9, -7.9	1.0	-11.76
Dysprosium II	4923	-8.8, -8.2	0.6	-10.90

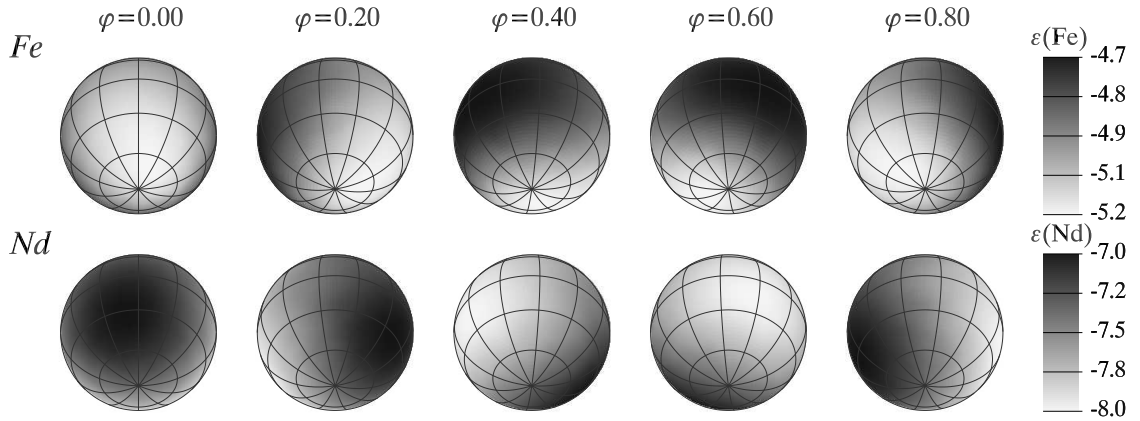


Figure 2: The abundance distributions of iron I and neodymium III on the surface of HD 24712. The upper panel shows the surface map of the iron I abundance and the lower panel presents the distribution of neodymium III. These maps were derived using the Stokes I and V parameter spectra as presented in Figure 3.

### 4.3 Surface abundances of individual elements

After having derived the magnetic field geometry of HD 24712 using the Fe I and Nd III lines, we could recover abundances of fourteen additional elements applying the INVERS10 code and the previously determined magnetic map during the various inversions.

#### 4.3.1 Magnesium, Calcium, and Scandium

The surface abundance distribution of *magnesium* was modelled using one Mg I line at 5528 Å with INVERS10, and we found a remarkable variation between  $-5.9$  and  $-4.3$  dex. *Magnesium* is, as scandium, titanium, iron, and nickel depleted (underabundant by up to 1.4 dex compared to the solar value) at the magnetic maximum phase, and shows a single, huge region of overabundance around the magnetic minimum, whereby the center of maximum abundance does not coincide with the (suspected) magnetic pole.

*Calcium*, in contrary to the other light elements that were mapped, shows its region of maximum abundance at the magnetic maximum phase, whereby the central region occupies latitudes higher than those for e.g. magnesium. We observe only a moderate variation between  $-5.2$  and  $-5.0$  dex.

*Scandium* exhibits a variation of 1.2 dex over the stellar surface, between  $-8.9$  and  $-10.1$  dex, also accumulated around the magnetic minimum, whereby the central region of maximum and also of the minimum abundance precedes that of magnesium by about  $60^\circ$ . The region of enhanced *scandium* abundance seems to occupy a larger fraction on the surface of HD 24712 than numerous other elements. At its maximum abundance phase, the *scandium* value corresponds to the solar one of 8.99 dex.

#### 4.3.2 Iron-peak elements

Three *titanium* II lines were used to recover the surface abundance structure of this element. As magnesium and scandium, it shows a tendency to accumulate near the magnetic minimum phase, exhibiting near solar concentration, and is depleted around the magnetic maximum, where abundance goes down to  $-7.8$  dex.

For *chromium* only one line around 5510 Å could be used as input for INVERS10 and we obtained a marginal variation between  $-5.9$  and  $-6.1$  dex. The general behaviour of this element

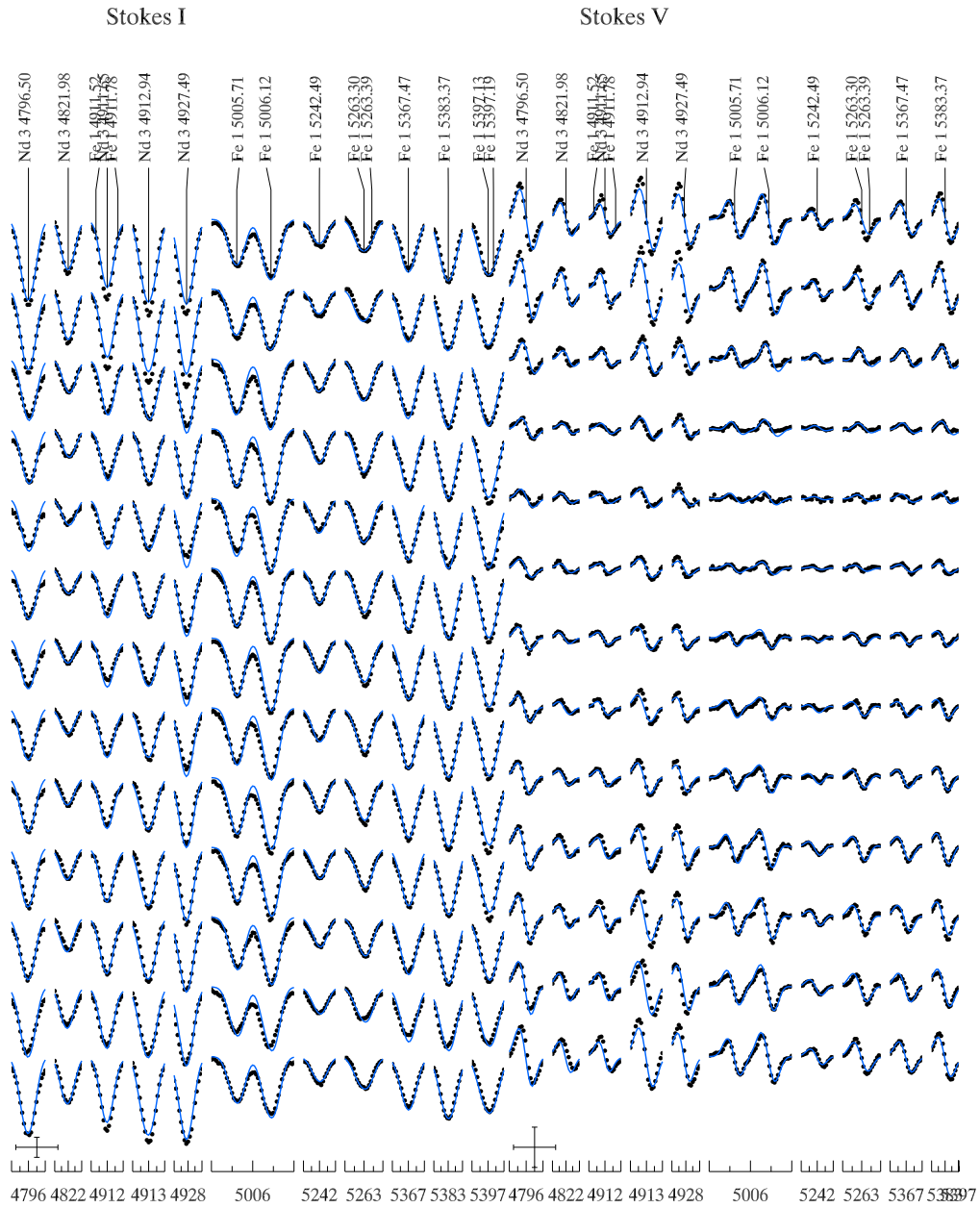


Figure 3: Comparison of the observed (dots) and calculated (lines) Stokes I and V profiles. Spectra are plot with increasing phase value (listed in Table 2) from top to bottom. The bars at the lower left and middle show the vertical and horizontal scale.

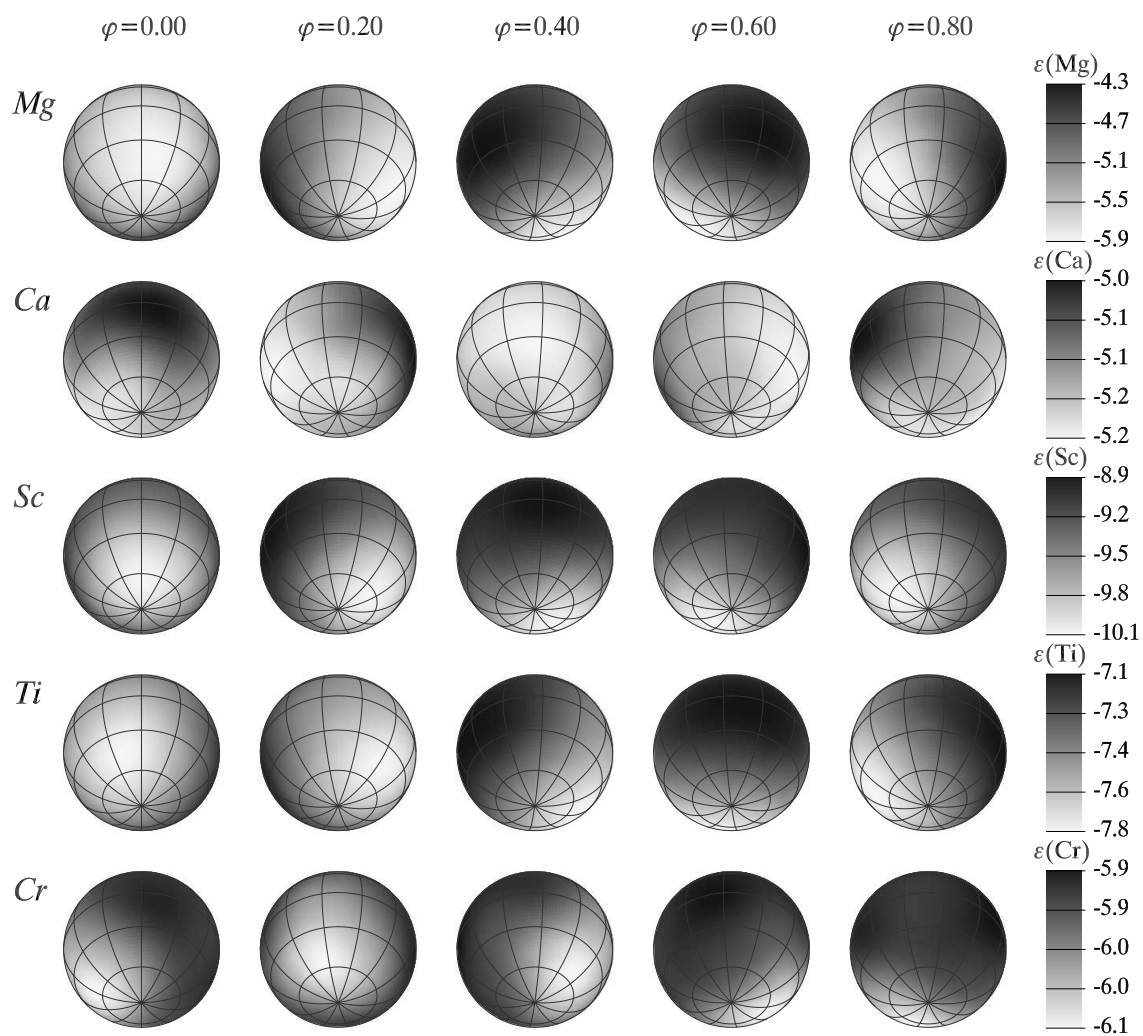


Figure 4: Abundance distribution of magnesium, calcium, scandium, titanium, and chromium on the surface of HD 24712 obtained from the lines listed in Table 3.

seems to correspond to that of Mg, Sc, Ti, and Fe, although the overall abundance varies only smoothly and very moderately from  $-5.9$  to  $-6.1$  dex (overabundant by up to  $-0.5$  dex compared to the solar value). The minima and maxima of iron abundance, as shown in our Figure 5 and described in Section 4.2, slightly, but noticeably precede the titanium extrema.

*Cobalt*, as calcium, yttrium, and all the REE, is clearly accumulated at the phase of magnetic maximum, and depleted around the minimum, varying between  $-5.8$  to  $-6.3$  dex and significantly overabundant with respect to the Sun ( $-7.12$  dex). The element was mapped taking into account six different cobalt I lines presented in Figure 6 and listed in Table 3.

A very interesting example of enormous line profile variation has been discovered for the *nickel* lines, nickel I at  $5035\text{\AA}$ , and  $5146\text{\AA}$ . The surface map revealed a huge, high contrast region of overabundance at phase 0.5 and a region of underabundance down to  $-7.6$  dex at the magnetic maximum phase. The line around  $5146\text{\AA}$  totally disappears at this rotational phase. Its distribution, in longitude and in latitude, is very similar to that of iron, and abundance varies from  $-7.6$  to  $-6.3$  dex, significantly underabundant compared to the solar value of  $-5.81$  dex. In order to check the abundance derived from the single  $5035\text{\AA}$  line and to be able to use the blend of Ni with Fe, Co, and Ce around  $5146\text{\AA}$ , we used the abundance pattern obtained from the Ni I  $5035$  line to map Co and Ce from the blend mentioned above, and got a very good agreement of observed and calculated profiles. The fit to the line profiles reached from this inversion is presented in Figure 6.

### 4.3.3 Yttrium and the rare-earth elements

*Yttrium* varies from  $-9.0$  to  $-8.5$  dex (overabundant up to  $1.3$  dex compared to the solar value of  $-9.83$ ), and exhibits a structure comparable to that of the REE, whereby the center of abundance is shifted to the northernmost part of the visible hemisphere and reaches its maximum and minimum, respectively, slightly after that of Nd. As presented in Figures 5, 7, and 8, ALL the REE we mapped are enhanced at the magnetic maximum phase and depleted where the magnetic field is at its minimum. We obtained abundances of Lanthanum, Cerium, of two different irons of Praseodymium and Neodymium, of Gadolinium, Terbium, and of Dysprosium.

*Lanthanum* is significantly overabundant compared to the solar value ( $-10.91$ ), and varies from  $-9.7$  to  $-8.8$  dex. It covers stellar latitudes very similar to those of Co, Nd, and Gd, whereby we would like to mention that, due to the very low  $v_e \sin i$  of the star, the latitudes of the abundance enhancement and depletion regions are affected by higher uncertainties than for stars with  $v_e \sin i$  higher than  $\simeq 10\text{ km s}^{-1}$ . The center of maximum abundance slightly lacks behind that of Nd.

The *Cerium* surface map was reconstructed using two different Ce II lines, also exhibiting the typical significant overabundance of REE in roAp stars of more than a dex, but varying only moderately over the surface between  $-9.3$  and  $-8.9$  dex. It is the first element that reaches its maximum abundance phase.

Singly and doubly ionized *Praseodymium* were mapped in separate inversions, as the doubly ionized REEs are significantly more abundant than the singly ionized components. It is not possible to fit line profiles of both ionization stages within the same inversion. Pr II was reconstructed using one line at  $5136\text{\AA}$ , and to derive Pr III, we could use two spectral lines around  $4910\text{\AA}$  and  $4929\text{\AA}$ . Pr II varies moderately between  $-10.0$  and  $-9.6$  dex. For Pr III we find abundances up to  $-7.7$  dex, compared to a solar value of  $-11.33$  dex. Praseodymium seems to be shifted in latitude relative to the neodymium enhancement region. This finding would help explaining the phase shift we found in our recent study (Ryabchikova et al. 2006) of radial velocity variations in high time resolved data obtained with the UVES spectrograph. There we find phase shifts between different radial velocity curves also from elements like e.g. Nd III and Pr III that should originate from comparable atmospheric depths and therefor NOT trace different pulsational phases, that usually lead to the

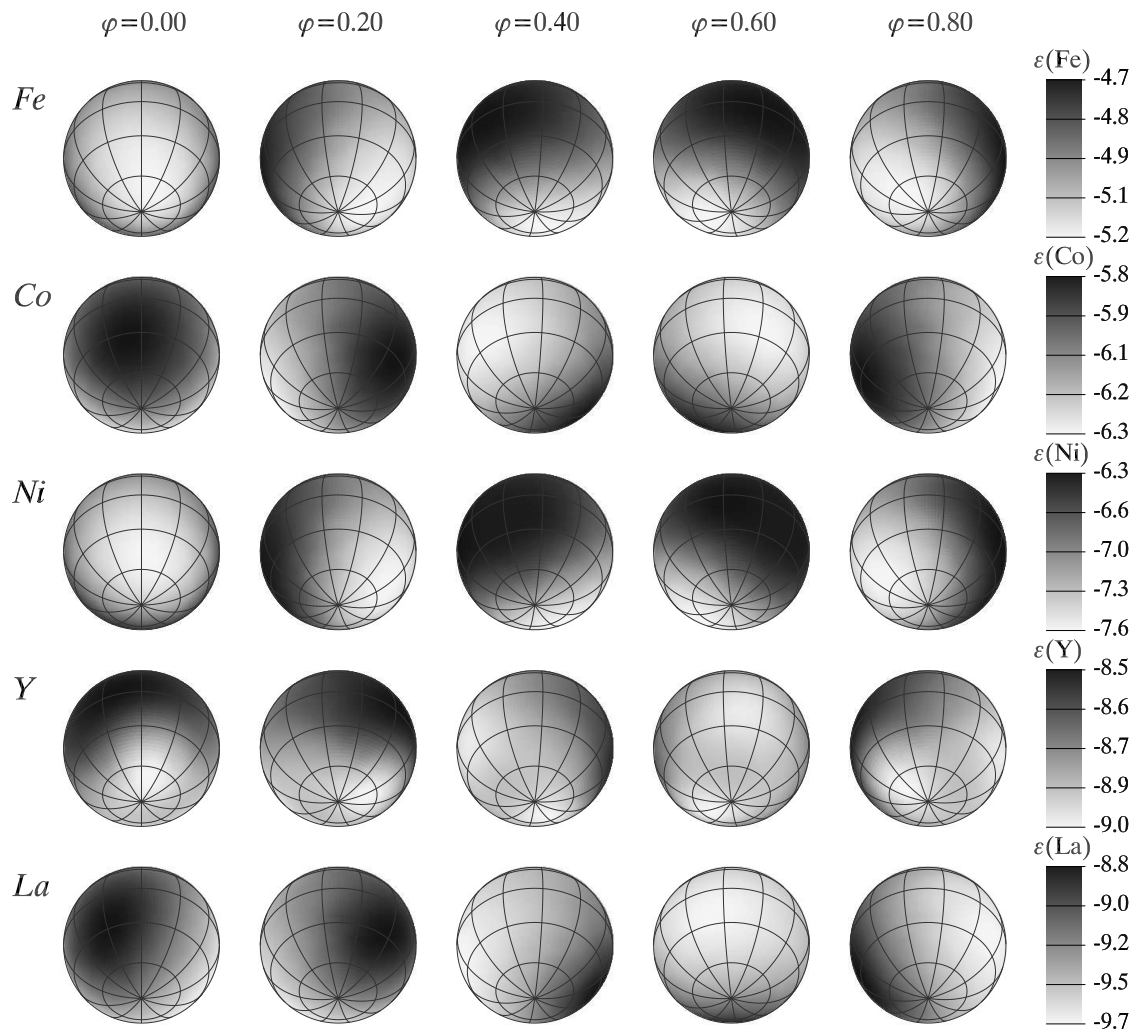


Figure 5: Surface abundance distribution of iron, cobalt, nickel, yttrium, and lanthanum (from top to bottom) on the surface of HD 24712. The maps were obtained taking into account the lines listed in Table 3.

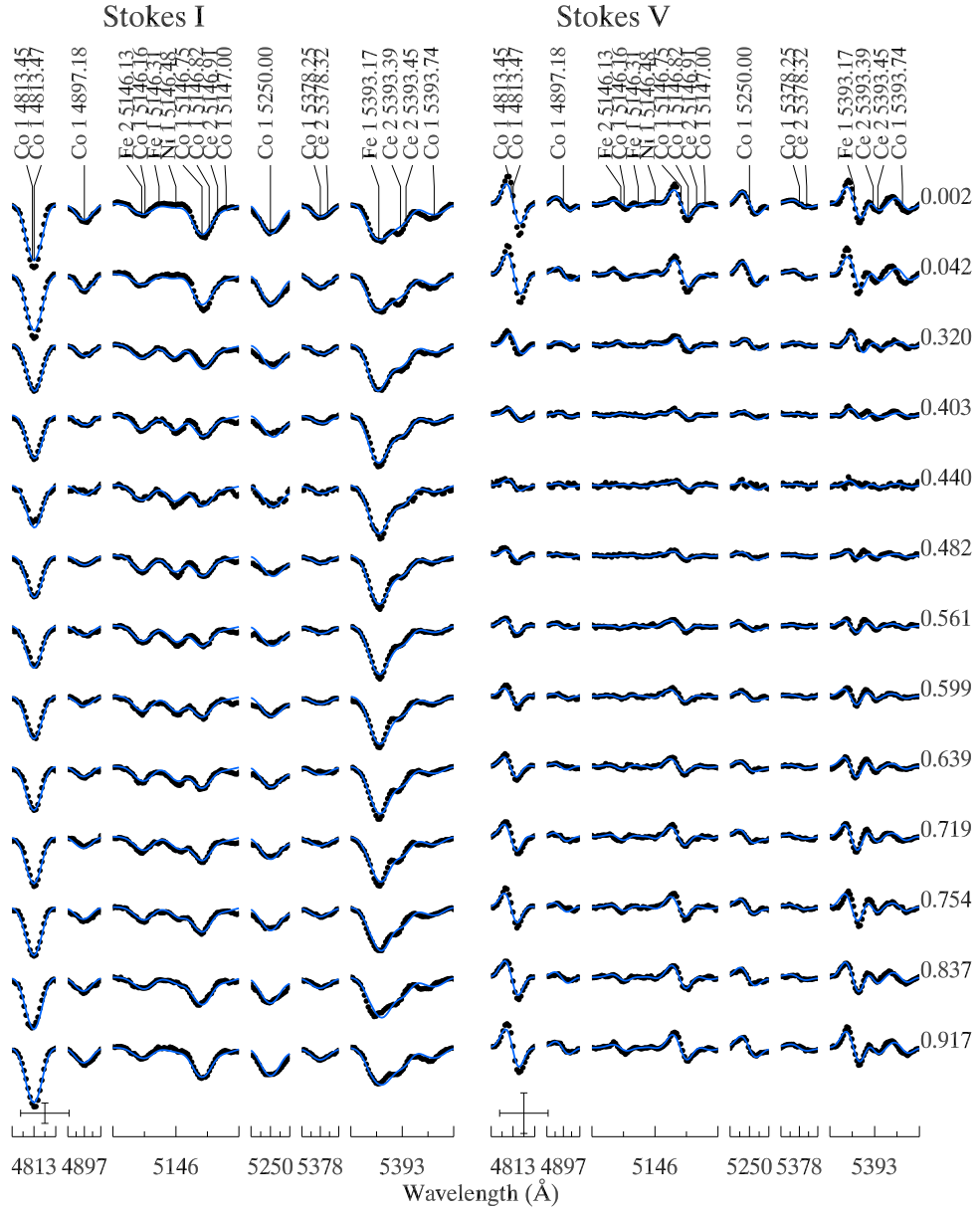


Figure 6: Comparison of the observed (dots) and calculated (lines) Stokes I and V profiles used for mapping of Co. Spectra are plot with increasing phase value (listed in Table 2) from top to bottom. The bars at the lower left and middle show the vertical and horizontal scale. Please note the total disappearance and reappearance of the Ni I line at 5146Å.

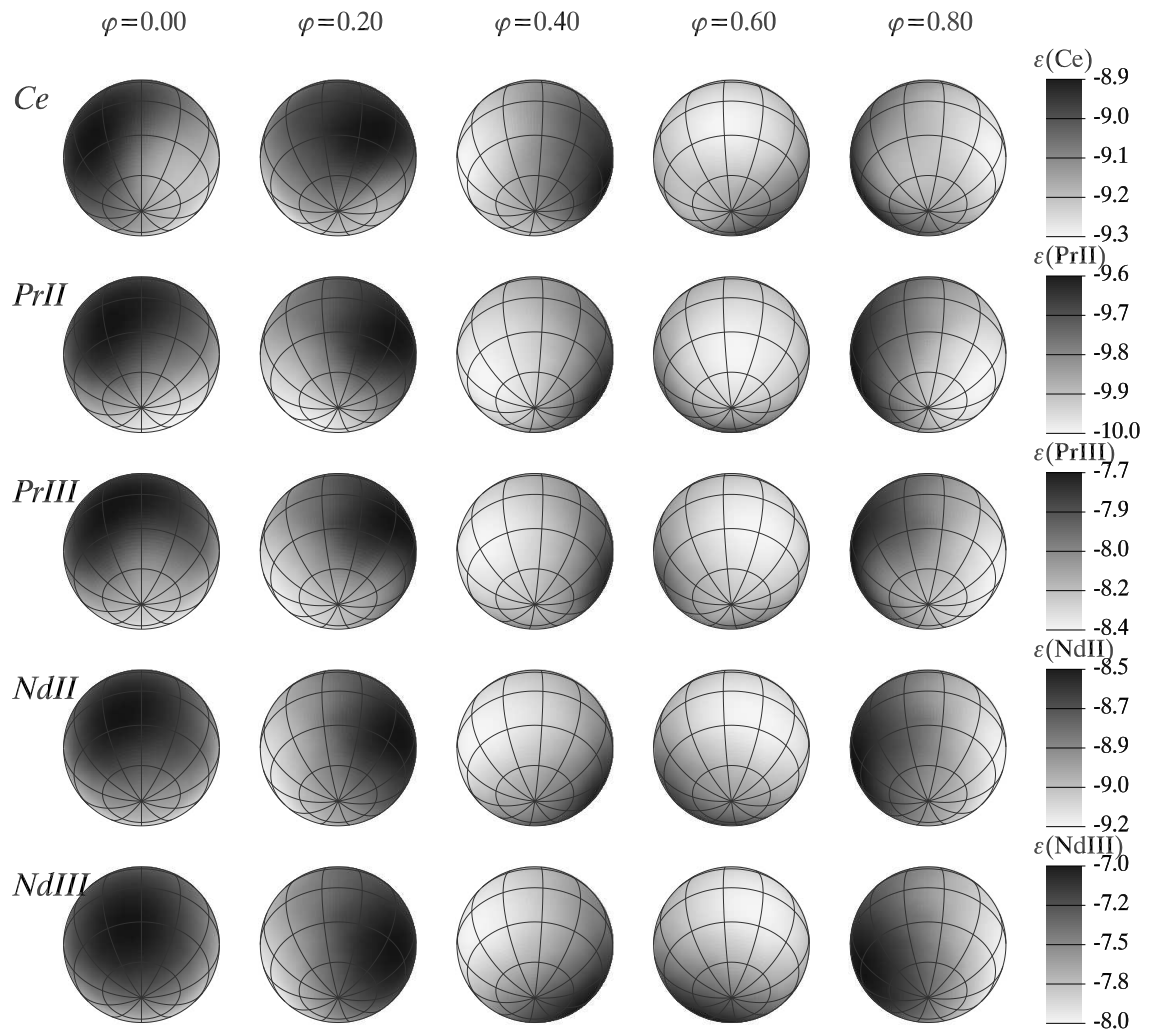


Figure 7: Elemental abundance distribution on the surface of HD 24712. Maps of cerium, praseodymium II and III, and of the first and second ionization stage of neodymium obtained from the lines listed in Table 3 are presented.

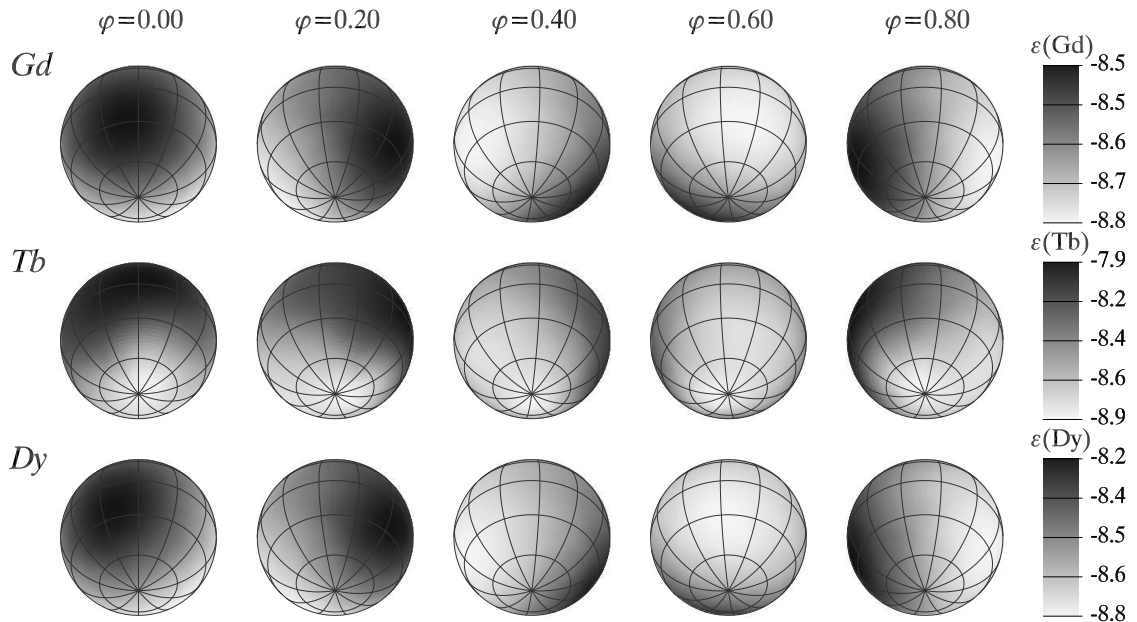


Figure 8: Surface abundance distributions of gadolinium, terbium, and dysprosium derived from the lines listed in Table 3.

observed phase shifts in radial velocity curves.

Abundances for *neodymium* were also derived considering singly and doubly ionized lines separately due to the huge abundance change between the different ionization stages. The Nd II surface map was derived from eight different lines listed in Table 3, and exhibits the same distribution as Nd III (described above), showing abundance variations from  $-9.2$  to  $-8.5$  dex, more than one dex below that of Nd III ( $-8.0$  to  $-7.0$  dex).

*Gadolinium* is concentrated in a spot very similar to that of neodymium, around the magnetic maximum phase, varying moderately between  $-8.5$  and  $-8.8$  dex, and is overabundant nearly up to 2.5 dex relative to the solar value of 10.92 dex.

Doubly ionized *Terbium* at  $5505\text{\AA}$  was used to map the surface distribution of this element, and it shows strong overabundance ( $-7.9$  dex) at the magnetic maximum phase compared to the solar value of  $-11.76$  dex. It is modulated between  $-8.9$  and  $-7.9$  dex, whereby the center of maximum abundance is shifted by  $\simeq 30^\circ$  to higher phases compared to Co, Nd, and Dy.

## 5 Conclusions

With the combination of spectropolarimetric observational data and magnetic Doppler Imaging we could derive, for the first time, the magnetic field geometry and abundances of numerous variable elements on the surface of a roAp star. We obtain a clear dipolar magnetic field structure and elemental abundance patterns, that are unexpectedly correlated to this geometry: instead of abundance enhancement regions on both magnetic poles or around the magnetic equator, we observe huge enhancement or depletion regions around either the phase of magnetic maximum or the magnetic minimum. In addition, these enhancement or depletion regions are shifted in latitude and longitude relative to each other, which might help us explaining the shifts in pulsational phases between elements like Pr and Nd, evident in the pulsation analysis of high time resolved spectroscopy (Ryabchikova et al. 2006; Sachkov et al. 2006, these proceedings). Furthermore the MOST light curve with changing amplitudes and asymmetries observed for different pulsational frequencies, most likely gives us information about magnetoacoustic effects in the atmospheres of

pulsating stars - although it is still unclear how to interpret this phenomenon. In an unprecedented combination of our various methods of analysing excellent observational data, we are able to obtain a detailed picture of the magnetic geometry on the stellar surface and of the extraordinary surface abundance variations and their relation to pulsational signatures and a 3D tomography of the stellar atmosphere, which will be obtained by relating optical depths to radial velocity amplitudes in our time resolved data.

Our analysis lead to a very complex picture of the interplay of magnetic field, pulsation, and atmospheric inhomogeneities in this roAp star, and we are able to provide, with the further development of theoretical aspects, new information for diffusion properties within the atmospheres of roAp stars, and to obtain new insights in the atmospheric structure and the geometry, origin, and interplay of abundance variations, pulsation and magnetic fields in this type of stars.

**Acknowledgements.** This work was supported by the Austrian Science Fund (FWF-PP17890).

## References

- Babel J., 1992, *Astron. Astrophys.*, **258**, 449  
 Bagnulo S., Landi Degl'Innocenti E., Landolfi M., Leroy J.L., 1995, *Astron. Astrophys.*, **295**, 459  
 Cunha M.S., Fernandes J.M.M.B., Monteiro M.J.P.F.G., 2003, *Mon. Not. R. Astron. Soc.*, **343**, 831  
 Cunha M.S., 2006, *Mon. Not. R. Astron. Soc.*, **365**, 153  
 Ilyin I.V., 2000, High resolution SOFIN CCD échelle spectroscopy, PhD Thesis, University of Oulu  
 Kochukhov O., Piskunov N.E., 2002, *Astron. Astrophys.*, **388**, 868  
 Kurtz D.W., 1982, *Mon. Not. R. Astron. Soc.*, **200**, 807  
 Kurtz D.W., Kawaler S.D., Riddle R.L., et al., 2002, *Mon. Not. R. Astron. Soc.*, **330**, L57  
 Matthews J.M., Wehlau W.H., Walker G.A.H., & Yang S., 1988, *Astrophys. J.*, **324**, 1099  
 Matthews J.M. et al., 2006, private communication  
 Piskunov N.E., Kochukhov O., 2002, *Astron. Astrophys.*, **381**, 736  
 Ryabchikova T. A., Landstreet J. D., Gelbmann M. J., Bolgova G. T., Tsymbal V. V., Weiss W. W., 1997, *Astron. Astrophys.*, **327**, 1137  
 Ryabchikova T.A., Tsymbal V.V., Malanushenko V.P., & Savanov I.S., 2000, in *Magnetic Fields of Chemically Peculiar and Related Stars*, eds. Yu. V. Glagolevskij, & I.I. Romanyuk, Moscow, 180  
 Ryabchikova T.A., Savanov I.S., Malanushenko V.P., Kudryavtsev D.O., 2001, *Astron.Rep.*, **45**, 382  
 Ryabchikova T., Nesvacil N., Weiss W.W., Kochukhov O., Stütz Ch., 2004, *Astron. Astrophys.*, **423**, 705  
 Ryabchikova T., Wade G.A., Aurière M., et al., 2005, *Astron. Astrophys.*, **429**, L55  
 Ryabchikova T., Sachkov M., Weiss W. W., Kallinger T., Kochukhov O., Bagnulo S., Ilyin I., Landstreet J. D., Leone F., Lo Curto G., Lüftinger T., Lyashko D., Magazzu A., accepted by *Astron. Astrophys.*, astro.ph.11848  
 Sachkov M., Ryabchikova T., Kochukhov O., Lyashko D., 2007, in: Proc. of Intern. Conf. "Physics of Magnetic Stars", eds. D.O. Kudryavtsev and I.I. Romanyuk, ???  
 Shulyak D., Tsymbal V., Ryabchikova T., Stütz Ch., Weiss W. W., *Astron. Astrophys.*, **428**, 993  
 Wolff S.C., Morrison N.D., 1973, *PASP*, **85**, 141  
 Walker G., Matthews G., Kuschnig R., et al., 2003, *PASP*, **115**, 1023